

Supporting Information

Experiment Section

Materials

Glycerol tripalmitate, poly(vinyl alcohol) (PVA), sodium chloride (NaCl), doxorubicin (DOX) hydrochloride, phosphotungstic acid, carbodiimide (EDC), N-hydroxysuccinimide (NHS), acetonitrile (CAN, HPLC-grade), porcine pancreatic lipase, colipase from porcine pancreas, paraformaldehyde, Superoxide Dismutase, methylthiazolotetrazolium and dimethyl sulfoxide (DMSO) were purchased from the Sigma-Aldrich Chemical Co. (St Louis, MO, USA). CdSSe/ZnS core/shell quantum dots (QDs) were obtained from Ocean Nanotech (Springdale, AR, USA). Hydrazine monohydrate was bought from Showa Chemical Industry Co. (Japan). Paclitaxel (PTX) was purchased from Scinopharm (Taiwan). All chemicals and solvents were of analytical reagent grade. DCFDA Cellular ROS Detection Assay Kit was purchased from Abcam (Cambridge, MA, USA). Glutathione Fluorometric Assay Kit and Superoxide Dismutase Activity Assay Kit were obtained from BioVision (Mountain View, CA, USA).

Preparation of the solid lipid spheres (SLSs)

The SLSs were fabricated by a modified double emulsion approach and the compositions of the system were summarized in Table 1. PVA was dissolved in all internal and external aqueous phases (W_1 , W_{21} and W_{22}) as a hydrophilic stabilizer. Sodium chloride (NaCl) was also dissolved in all aqueous phases to adjust the osmotic pressure. The process was detailed as follows:

- (1) Primary emulsification: 100 μ L of 1 % (w/v) PVA and 0.1 % NaCl solution (W_1) was first prepared as the internal aqueous phase and added into 1000 μ L of chloroform and ether solvent (1:1), which pre-dissolved 5 mg Glycerol tripalmitate. The mixed solution was subsequently emulsified at 40 W using an

ultrasonic processor (Hielscher, Germany).

- (2) Secondary emulsification: The obtained emulsion was followed by emulsifying again at 100 W in 3 mL of a 1 % PVA and 0.1 % NaCl solution (first external aqueous phase, W_{21}) to form primary W/O/W emulsion solution.
- (3) Osmotic deswelling: Sequentially, the primary emulsion solution was added into the second external aqueous phase (W_{22}) with different concentrations of PVA or NaCl (volume ratio 3). After the gentle stirring, a large osmotic pressure difference between W_1 and W_{22} was generated and resulted in fast deswelling of entrapped W_1 droplet.
- (4) Collection: The organic solvent was removed using a rotary vacuum evaporator (Eyela, Japan) and the SLSs were precipitated and redispersed in aqueous solution. To remove the excess surfactants, the SLSs were washed three times by centrifuging at 8000 rpm and were concentrated to 5 mL with deionized water.

Characterization of SLSs

The average size and zeta potential of the samples were measured by dynamic light scattering (Delsa Nano C, Beckman Coulter, USA). The nanostructure of the SLSs was observed by transmission electron microscopy (TEM) (JEM-2100F, Japan). After being negatively stained by 2% phosphotungstic acid (PTA) solution, a droplet of the samples was dropped on a Lacey Cu grid and dried at room temperature. The shell thickness of the SLSs was calculated from TEM micrographs. Each thickness was averaged statistically by thirty nanoparticles.

Enzyme-responsive degradation by lysosomal acid lipase and drug release

Lysosomal acid lipase (LAL)-mediated degradation assay was performed based on the method described in our previous study ¹. Briefly, the lipase/colipase complex was first prepared by mixing 600 μ L lipase solution (2000 U mL^{-1}) and 360 μ L of colipase solution (50 $\mu\text{g mL}^{-1}$) and then incubated at 37 °C for 15 min. Subsequently, the

complex solution was reconstituted using citrate buffer (0.1 M) at pH4.8 (the pH value of lysosomal content) and 10 mg of the SLSs with varying shell thickness were severally added into the LAL suspension at 37 °C with magnetic stirring to initiate the degradation reaction. After incubation for 12 h, 10 µL aliquots of the mixture were drawn and negatively stained by 2% PTA solution. A droplet of the samples was then dropped on a Lacey Cu grid and observed using TEM. To quantify the degradation degree of the SLSs, 50 µL aliquots of the mixture were drawn and analyzed using Non-esterified free acid (NEFA) assay kit (Wako Diagnostics, Richmond, VA, USA) at predetermined time points. Colorimetric changes related to concentrations of free fatty acids were measured using Sunrise absorbance microplate reader at 550 nm with oleic acid (OA) as a standard. The fatty acids released from the lipid nanoparticles were quantified and expressed in terms of the percentage of fatty acids that can possibly be freed after complete degradation. The release of the entrapped OA and formation of free fatty acids from LAL enzymatic degradation of the triglyceride components were all included,² and the experiments were performed in triplicate.

Preparation of QD-DOX, LS/QD, LS/QD-SOX and PLS/QD-DOX

Synthesis of quantum dot-doxorubicin conjugates (QD-DOX) was performed based on a previously described method³. Briefly, one nanomole of QD-COOH dispersed in 875 µL of anhydrous dimethyl sulfoxide were mixed with 50 µL of 50 mM EDC and 25 µL of 25 mM NHS with gentle stirring for 15 min. Then, 32 µL of hydrazine monohydrate (80% v/v) was added into the solution. After reacting for 3 h at room temperature under stirring, the solution was diluted to 3 mL using H₂O and washed by centrifuging three times at 13000 rpm. The solution was then concentrated to 500 µL. 100 µL of DOX (10 mg/mL) and 600 µL of anhydrous DMSO were added into the solution for 48 h of reaction. After the reaction completed, the mixture was diluted to 3 mL with H₂O, washed by centrifuging three times at 13000 rpm and concentrated to

1 mL with H₂O.

The composition of LS/QD (QD-loaded), LS/QD-DOX (QD-DOX loaded) and PLS/QD-DOX (PTX and QD-DOX loaded) were similar to the SLSs, but the internal aqueous phase W₁ contained 1 nmole QD (LS/QD) or QD-DOX (LS/QD-DOX and PLS/QD-DOX), respectively, along with 1 % PVA, 0.1 % NaCl solution. Besides, 0.5 mg PTX was also dissolved in the organic solvent of PLS/QD-DOX. The rest of the composition and procedure was the same as the process as described above.

Quantification of conjugated DOX and hydrolytic release test

The amount of conjugated DOX on the QD was determined using ultraviolet (UV) absorption at a wavelength of 480 nm, a strong absorption band of DOX, with reference to a calibration curve on a UV-Vis spectrometer (Agilent, 84531 UV-Visible spectrophotometer). QDs solution with the same concentration was used as a reference.

To investigate the DOX release from QD-DOX, the QD-DOX was dispersed in phosphate buffered saline (PBS) with pH 4.8. At pre-determined time points, aliquots of samples were taken from the bulk solution and centrifuged at 13000 rpm in Amicon Ultra Centrifugal Filter Unit (molecular weight cutoff of 10 kDa) for three times to remove released DOX. The concentration of remaining DOX in the samples was determined using UV-Vis spectrometer. Besides, the fluorescent spectrum at 480 nm of QD in the samples was also detected using Hitachi F-4500 fluorescence spectrophotometer (Japan).

Encapsulation efficiency of PLS/QD-DOX

Encapsulation efficiency (EE) of PLS/QD-DOX carriers was examined using both UV spectroscopy and high-performance liquid chromatography (HPLC) method. The samples were first washed by EtOH/water (50%, v/v) and the solution was centrifuged at 8000 rpm for 10 min. The supernatant was then measured using UV

spectrometer to determine the amount of un-encapsulated DOX. Subsequently, the PTX in the EtOH/water solution was extracted with chloroform and re-dispersed in 50% ACN after drying in an oven at 60°C. The amount of PTX was quantified using HPLC (Agilent Technologies 1200 series) with a 4.6 x 150 mm ZORBAX Eclipse XDB-C18 (5µm) column. The detector was operated at a wavelength of 290 nm, and the sample was eluted using a mobile phase composed as follows: A=40 % deionized water and B=60 % (ACN). The EE of the PTX and DOX in the PLS/QD-DOX was calculated as follows:

$$EE = \left[\frac{(W_i - W_f)}{W_i} \right] \times 100 \%$$

where W_i is the initial amount of PTX or DOX, and W_f is the amount of un-encapsulated PTX or DOX in the supernatant.

Kinetics study of the released PTX and DOX in a simulated lysosomal environment

A release kinetics study of the encapsulated PTX and DOX from PLS/QD-DOX was performed using a modified experimental procedure. The mixture of 200 µL suspension containing 10 mg PLS/QD-DOX and 2300 µL LAL suspension was added to a dialysis tubing cellulose membrane with a cutoff molecular weight of 12,000. The dialysis bags were dialyzed in release medium (1 % Tween-80 (v/v) in deionized water) at 37 °C with gentle shaking, and aliquots of incubation medium were collected at predetermined time points. The amounts of released drugs were quantified using both UV spectroscopy and HPLC method. The solution was maintained at a constant volume by replacing original solution with release medium. All experiments were performed in triplicate.

Subcellular localization and executive stage of the PLS/QD-DOX

DOX-resistant (MCF-7/ADR) human breast carcinoma cells were kindly provided by Professor Ming-Jium Shieh (National Taiwan University, Taiwan) and grown in

75T culture flasks in DMEM culture medium supplemented with 10% FBS and 1% penicillin–streptomycin–neomycin solution at 37 °C under 5% CO₂. The cells were continuously maintained in 0.5 μM DOX. In confocal laser scanning microscope (CLSM) experiment, MCF-7/ADR cells were seeded on 22-mm² glass coverslips placed in 6-well plates. After incubation for 24 h, PLS/QD-DOX was added into each well at a concentration of 20 μg mL⁻¹. After 12h and 18 h, the cells were harvested and washed several times with PBS. The cells were then fixed with 3.7% paraformaldehyde solution and stained by DAPI. Subcellular localization and executive stage of PLS/QD-DOX were investigated using confocal laser scanning microscope (CLSM, D-Eclipse C1, Nikon, USA).

Assessment of ROS generation and oxidative stress biomarkers

The ROS generation and oxidative stress induced by LS/QD (30 nm shell thickness) were assessed by measuring the concentration of ROS, Glutathione (GSH), Glutathione disulfide (GSSG) and activity of superoxide dismutase (SOD) in MCF-7/ADR cells. The concentration of ROS, GSH, GSSG and SOD was determined by the commercially available kits based on the method provided by the manufacturer. The cells were cultured in a 96 well plate with density of 2.5 x 10⁴ per well (for ROS assay) and 6 well plate with density of 2 x 10⁶ per well (for GSH and SOD assay), respectively, and exposed to different concentrations of LS/QD. After incubation for 24 and 48 h, the cells were harvested and assayed following the instructions supplied with the commercial kits. The result of ROS evaluation was expressed as % increase of DCF fluorescence intensity compared to untreated control. The concentration of GSH was expressed as nmole/mg protein and SOD activity was expressed as U/mg protein.

Assays of cellular cytotoxicity

In vitro cytotoxicity of free drugs, free QD, single drug-loaded, single drug and

QD-loaded, dual drug-loaded and dual drug and QD-loaded carriers were examined on MCF-7/ADR cells using methylthiazolotetrazolium (MTT) method. 10^4 cells per well were first seeded in 96-well plates and exposed to serially equivalent drug concentrations (PTX or DOX or PTX and DOX) of free drugs, single drug-loaded carriers, single drug and QD-loaded carriers, dual drug-loaded carriers and dual drug and QD-loaded carriers at 37 °C for 48 h. The molar ratio of PTX : DOX is 2:1 in dual drug-loaded carriers (with or without QD) and the concentration of QD was constant (200 nM) in every drug concentration. Subsequently, 20 μ L of MTT solution (5 mg mL⁻¹ in PBS, pH 7.4) was added, and the cells were incubated for an additional 4 h. The medium was replaced with 200 μ L of DMSO, and the absorbance was monitored using a Sunrise absorbance microplate reader at the wavelength of 595 nm. Finally, the cell viability was determined by comparison with untreated control and calculated using the following equation:

$$\text{Cell Viability (\%)} = (A_{\text{sample}} / A_{\text{control}}) \times 100\%$$

The half maximal inhibitory concentration (IC₅₀), which is defined as the dosage of a compound that inhibited 50% of cell growth, was calculated from the obtained viability curves using CompuSyn software (Version 3.0.1, 2007, ComboSyn Inc., Paramus, NJ). All experiments were performed in triplicate. For the cytotoxic assay of PLS/QD-DOX with different shell thickness, same procedure was adopted, but the cells were incubated with the PLS/QD-DOX for 18 h and 36 h before harvest.

Figures

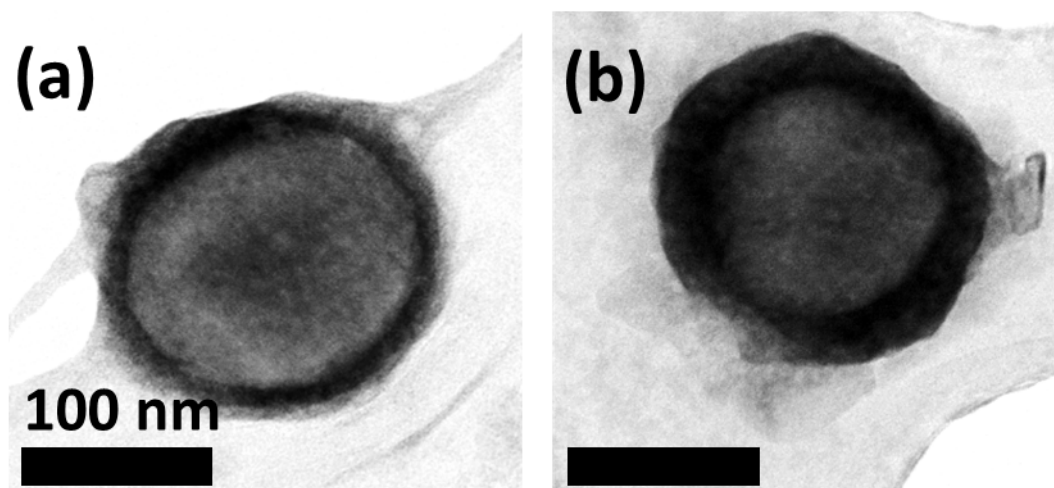


Figure S1. TEM images of the SLSs fabricated with 1% PVA and (a) 1M or (b) 2 M NaCl in the external aqueous phase W_{22} . As shown in Figure S1 and 2a–d, increasing the concentrations of NaCl and PVA led to an increase in the shell thickness and a decrease of internal droplet volume. However, in our study PVA concentration could cause more significant change. It might be attributed to the following two reasons: (i) the osmotic gradient induced by PVA concentration was stronger and more predominant than that induced by NaCl concentration. (ii) PVA acted as a surfactant to stabilize the hydrophobic phase of the emulsion dispersing in the aqueous phase. Therefore, as increasing PVA concentration in W_{22} , hydrophobic phase of the emulsion would become more stable and enable to accommodate more lipids, resulting in a thicker shell of the carrier.

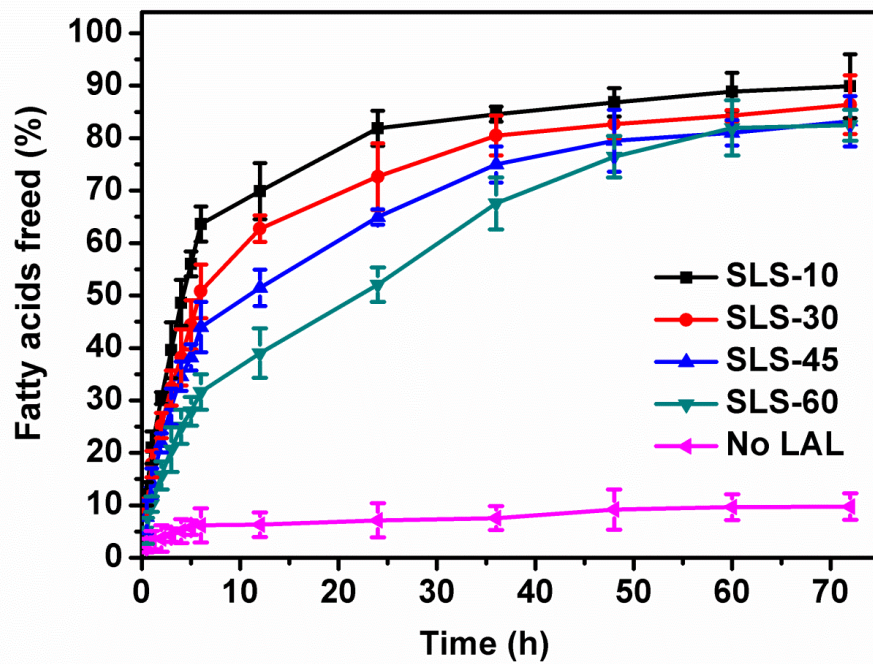


Figure S2. The degradation profiles of SLS with varying shell thickness (10, 30, 45, 60 nm) at 37 °C in the presence and absence (no lysosomal acid lipase) of lysosomal acid lipase (LAL) buffer. These results showed a positive correlation between the degree of degradation with the thickness of the lipid shell, which agreed with the TEM observations.

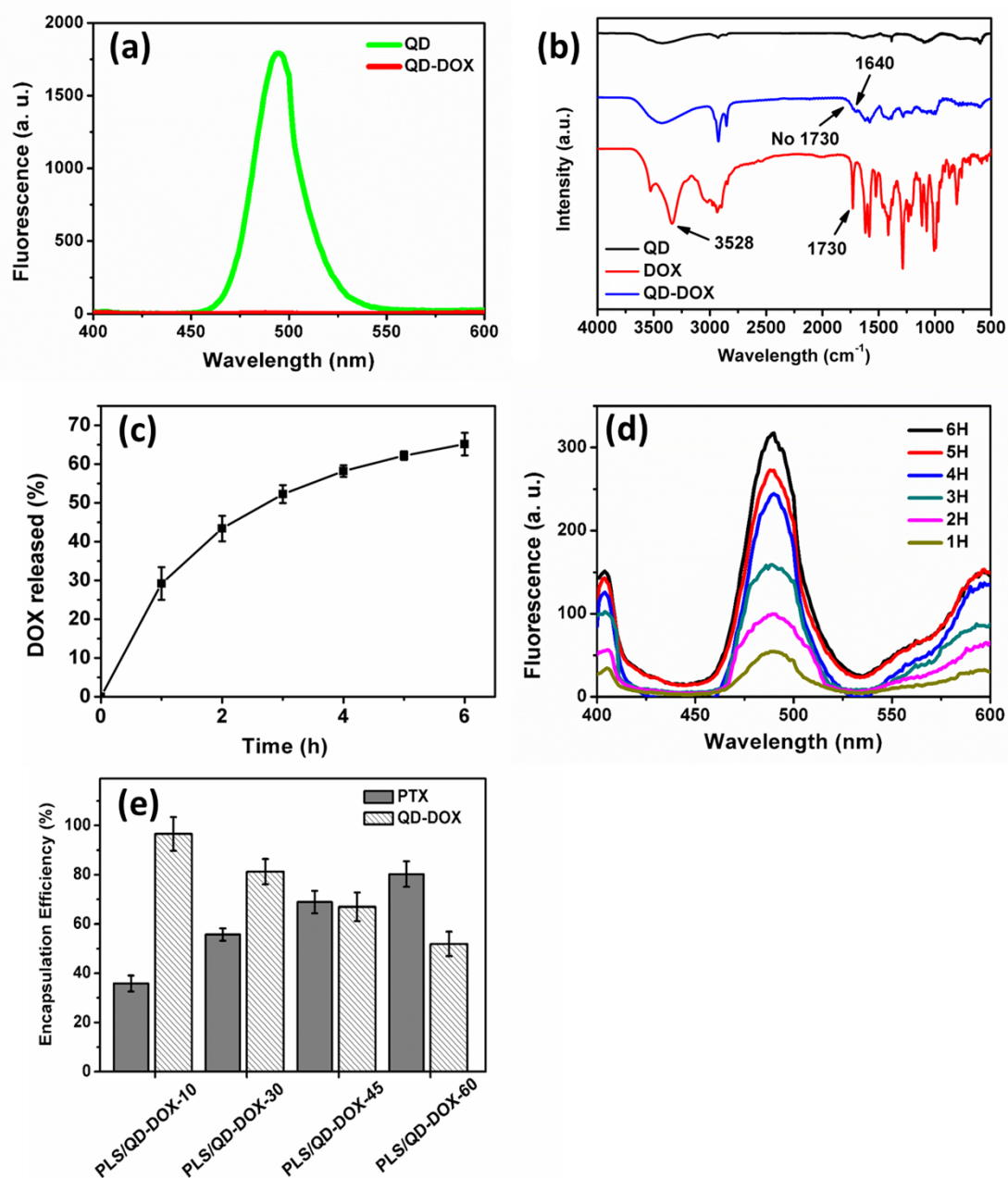


Figure S3. Characterization of QD-DOX. In order to develop a Förster resonance energy transfer (FRET) indicator and pH-responsive release of DOX in the lysosomes, carboxyl-terminated QD were conjugated with DOX using a pH-sensitive hydrazone bond, which is stable at neutral pH but easily broken at low pH.⁴ There were approximately 196 DOX molecules bound on a QD molecule according to the calculation from a standard curve made by absorbance of predefined DOX concentrations. (a) The quenching of QD fluorescence was substantiated by a direct measurement of fluorescence of un-conjugated QD and QD-DOX using the 390 nm excitation, indicating that FRET phenomenon occurred between QD and DOX when their distance was short enough (< 10 nm). (b) The Fourier transform infrared (FTIR)

spectra of the QD-DOX. The formation of a hydrazone bond could be demonstrated by the appearance of a characteristic imine peak (C=N) at 1640 cm^{-1} and the disappearance of the peak at 1730 cm^{-1} due to the carbonyl stretching frequency of free DOX.^{5, 6} The peak at 3528 cm^{-1} is attributed to O-H group. In addition, (c) the release of DOX from QD-DOX and (d) the recovery of QD fluorescence in an acidic environment (pH=4.8, the pH value of lysosomal content) were further examined. It was found that 65% of conjugated DOX was released from QD-DOX after 6 h of incubation and at the meantime, the QD fluorescence also restored increasingly as the FRET quenching effect disappeared. The results demonstrate that the DOX release could be indicated by chromatic transduction of fluorescent signal, which was used as an FRET indicator to exhibit executive stage of PLS/QD-DOX in the following experiments. (e) PTX and QD-DOX EE of the PLS/QD-DOX carriers (named after shell thickness— 10, 30, 45, 60 nm) was highly related to the volume of lipid shell and internal droplet phase. PTX EE of PLS/QD-DOX named after their thickness (10, 30, 45, 60 nm) was 35.83 ± 3.25 , 55.73 ± 2.51 , 68.92 ± 4.58 and 80.24 ± 5.15 %, respectively, because more space was available for the carrier with thicker shell to accommodate the hydrophobic drug. On the other hand, the corresponding QD-DOX EE with increasing shell thickness were 96.53 ± 6.82 , 81.27 ± 5.14 , 66.94 ± 5.83 and 51.87 ± 4.98 %, respectively, which showed opposite tendency to PTX EE. It was likely because the carrier with thicker shell has a smaller inner droplet phase which was capable of accommodating limited amount of QD-DOX. The results suggested that the relative drug loading ratio of PTX and QD-DOX can be controlled by adjusting the shell thickness and inner droplet volume of the PLS/QD-DOX.

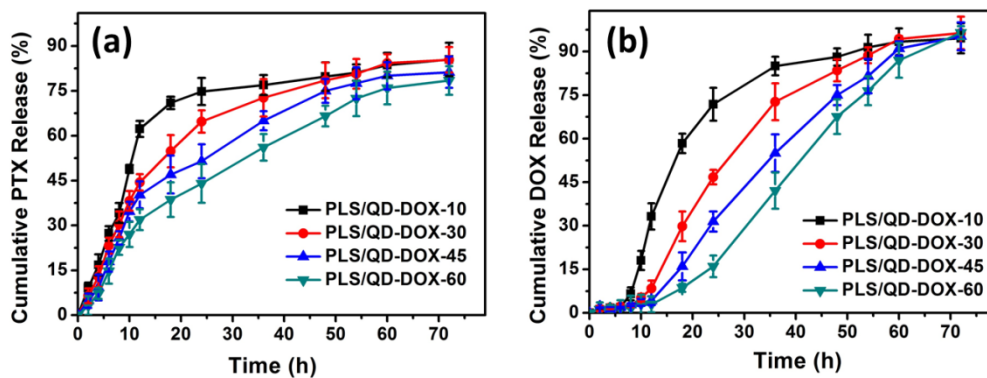


Figure S4. Kinetic studies of (a) PTX and (b) DOX release by LAL when incubating the PLS/QD-DOX carriers in simulated lysosomal environment for at 37 °C. Over 60% of PTX was cumulatively released from PLS/QD-DOX-10 within 12 h (Fig. S4a), most likely due to the faster collapse of the thinner lipid shell in the presence of lipase. However, the percentage of released PTX decreased as the shell thickness of the carriers increased. This trend could be understood in terms of the lower degradation degree and higher PTX-loading amount. In contrast, DOX showed a similar release profile but exhibited a delayed threshold within 0-10 h, depending on the shell thickness (Fig. S4b). This delayed threshold again indicated that the DOX would not release until the lipid shell was degraded and the hydrazone bond of the QD-DOX conjugate was broken.

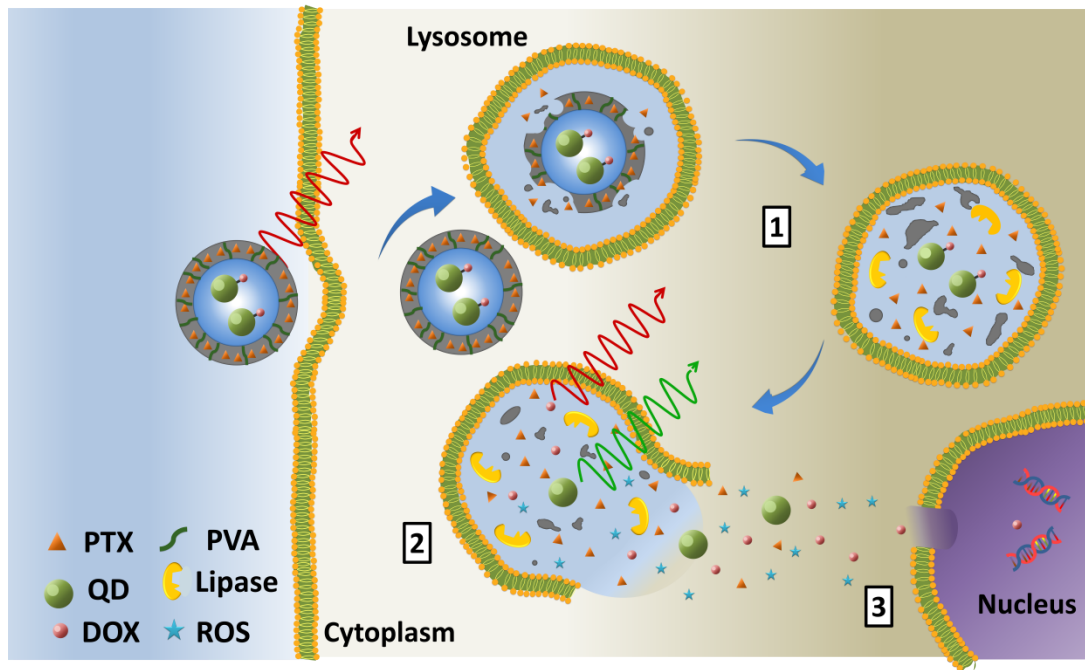


Figure S5. The schematic illustration represented the executive stage of PLS/QD-DOX, including: (1) degradation of lipid shell, release of PTX, and display of DOX fluorescent; (2) release of DOX and display of both DOX and QD fluorescence; (3) production of ROS and induction of cell death. This easily detectable manner of fluorescent transduction can be used to indicate delivery pathway of the carrier and release of the therapeutic modality.

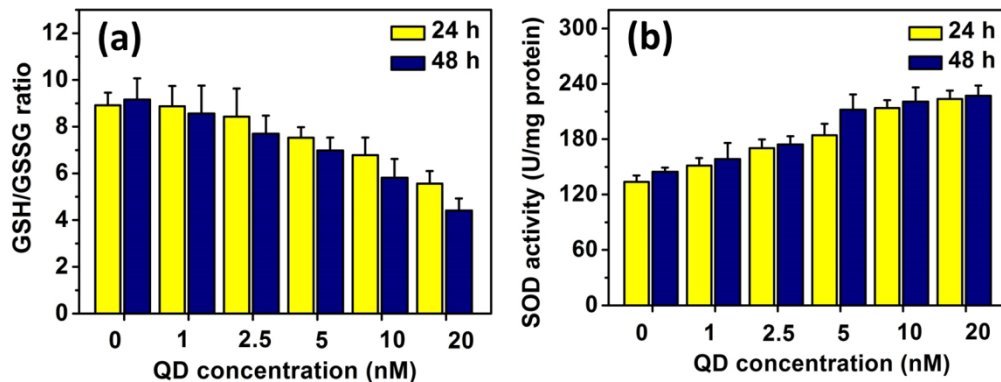


Figure S6. The evaluation of biomarkers of oxidative stress in MCF7/ADR cells after incubation with varying concentrations of the QDs. (a) GSH/GSSG ratio and (b) SOD activity revealed oxidative condition of the cells. GSH is an essential antioxidant involved in the ROS detoxification pathway and oxidized to form a GSSG disulfide during oxidative stress. Alteration in GSH level content is regarded as an indication of adaptive response of the cell to abnormal oxidative condition.⁷ In aerobic organisms, SOD is responsible for catalyzing the dismutation of superoxide radical to form hydrogen peroxide,⁸ which can be further decomposed to produce H₂O. The experiments were performed in triplicate and shown in means \pm SD.

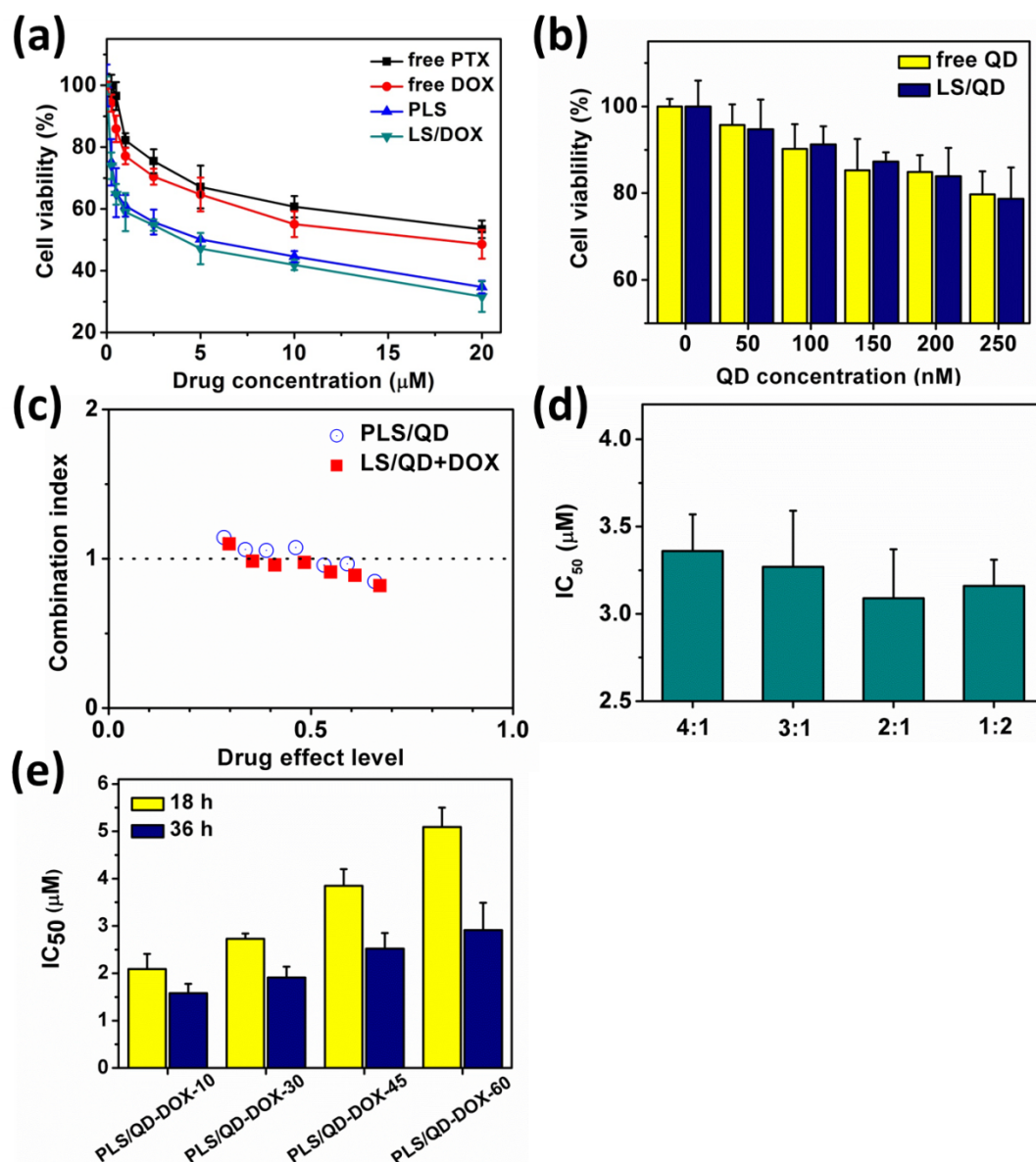


Figure S7. Cellular viability of MCF-7/ADR cells treated with (a) free drugs, carrier forms (PLS and LS/QD), (b) free QD and QD carrier (LS/QD) for 48 h. It was found that both the carriers of PTX and DOX showed more cytotoxicity than that of free drugs, but no obvious difference was observed between free QD and QD-loaded carriers. This result occurred because PTX and DOX are substrates of P-glycoprotein, which is an efflux pump over-expressed in the MCF-7/ADR cells that is regarded to be responsible for multidrug resistance in cancer cells.⁹ (c) The synergistic effect of combination therapy of QD-loaded carriers with PTX (PLS/QD) or DOX (LS/QD+DOX) was statistically analyzed using CompuSyn software. Combination index (CI) is a quantitative measure of the degree of drug interaction in terms of synergism ($\text{CI} < 1$), additive effect ($\text{CI} = 1$) and antagonism ($\text{CI} > 1$) for a given endpoint of the effect measurement. (d) The IC_{50} values of different molar ratios of PTX and

DOX in the carrier (PTX : DOX=1:2, 2:1, 3:1 and 4:1). (e) The IC₅₀ values of PLS/QD-DOX carriers after incubation for 18 h and 36 h were compared to investigate the influence of the shell thickness on cytotoxicity. According to the abovementioned data, shell thickness of PLS/QD-DOX had a critical influence on both drug loading and release rate, so we postulated the intracellular behavior of the PLS/QD-DOX might be related to the shell thickness as well. Before encapsulated into the carrier, DOX was pre-conjugated to QD, and there were approximately 196 DOX molecules bound on a QD. EE of PLS/QD-DOX-10, 30, 45 and 60 were determined in previous experiment and the corresponding molar ratio of PTX : DOX is 1:2, 2:1, 3:1 and 4:1, respectively. The IC₅₀ values showed a thickness-dependent tendency and the potency were lower for the carriers with thicker shell. It was inferred that the carrier with thinner shell contained more QD amount, which increased the potency predominantly. Moreover, it was noteworthy that the IC₅₀ diminishment of the PLS/QD-DOX-10, 30, 45, and 60 between 18 h and 36 h were 0.51, 0.82, 1.33 and 2.18 μM, respectively. There was more significant time-dependent cytotoxicity on the PLS/QD-DOX-45 and PLS/QD-DOX-60 treatment group because their DOX just started to release at first 18 h and had not yet arrived at the nucleus according to the results of CLSM. The enhanced cytotoxicity after treatment of 36 h demonstrated that the encapsulated drug had released completely. In contrast, most of the encapsulated drug in the carriers with thinner shell (PLS/QD-DOX-10 and PLS/QD-DOX-30) had been released, so more cells were killed under the synergistic effect of dual drug and oxidative stress at the first 18 h.

Tables

	NaCl concentration in W ₂₁ (M)	NaCl concentration in W ₂₂ (M)	PVA concentration in W ₂₁ (%)	PVA concentration in W ₂₂ (%)	Mean size (nm)	PDI	Thickness (nm)	Zeta Potential (mV)
1	0.1	0.5	1	1	178.7 ± 9.6	0.183 ± 0.055	11.6 ± 3.9	1.6 ± 0.5
2	0.1	1	1	1	175.2 ± 6.8	0.274 ± 0.095	18.9 ± 2.8	0.9 ± 0.3
3	0.1	2	1	1	171.3 ± 5.7	0.169 ± 0.105	24.7 ± 4.9	2.7 ± 0.9
4	0.1	2	1	2	167.6 ± 8.6	0.215 ± 0.084	30.7 ± 8.8	0.7 ± 0.8
5	0.1	2	1	3	161.4 ± 5.5	0.145 ± 0.034	44.0 ± 9.7	3.4 ± 1.2
6	0.1	2	1	4	155.9 ± 6.9	0.194 ± 0.074	62.5 ± 13.3	2.5 ± 0.3

Table S1. Mean size, PDI, thickness and zeta potential of the SLSs with different compositions.

Reference

1. C. W. Su, S. Y. Chen and D. M. Liu, *Chem. Commun.*, 2013, **49**, 3772-3774.
2. P. Nilssonhle, A. S. Garfinkel and M. C. Schotz, *Annu. Rev. Biochem.*, 1980, **49**, 667-693.
3. R. Savla, O. Taratula, O. Garbuzenko and T. Minko, *J. Controlled Release*, 2011, **153**, 16-22.
4. T. Etrych, M. Jelinkova, B. Rihova and K. Ulbrich, *J. Controlled Release*, 2001, **73**, 89-102.
5. Z. Xu, K. Zhang, C. Hou, D. Wang, X. Liu, X. Guan, X. Zhang and H. Zhang, *Journal of Materials Chemistry B*, 2014.
6. J. Zhang, X. Lin, J. Liu, J. Zhao, H. Dong, L. Deng, J. Liu and A. Dong, *Journal of Materials Chemistry B*, 2013, **1**, 4667-4677.
7. D. Pezzoli, M. Zanda, R. Chiesa and G. Candiani, *J. Controlled Release*, 2013, **165**, 44-53.
8. C. I. Jones, H. Zhu, S. F. Martin, Z. S. Han, Y. B. Li and B. R. Alevriadou, *Ann. Biomed. Eng.*, 2007, **35**, 683-693.
9. K. Thanki, R. P. Gangwal, A. T. Sangamwar and S. Jain, *J. Controlled Release*, 2013, **170**, 15-40.